POLITECNICO DI TORINO
Repository ISTITUZIONALE

Progressive damage analysis of composite laminates subjected to low-velocity impact using 2D layer-wise structural models

Original
Progressive damage analysis of composite laminates subjected to low-velocity impact using 2D layer-wise structural models / Nagaraj, M.H., Carrera, E., Petrolo, M.. - In: INTERNATIONAL JOURNAL OF NON-LINEAR MECHANICS. - ISSN 0020-7462. - ELETTRONICO. - 127:(2020). [10.1016/j.ijnonlinmec.2020.103591]

Availability:
This version is available at: 11583/2843331 since: 2020-08-31T08:37:11Z

Publisher:
Elsevier

Published
DOI:10.1016/j.ijnonlinmec.2020.103591

Terms of use:

This article is made available under terms and conditions as specified in the corresponding bibliographic description in the repository

Publisher copyright
Elsevier postprint/Author's Accepted Manuscript

© 2020. This manuscript version is made available under the CC-BY-NC-ND 4.0 license
http://creativecommons.org/licenses/by-nc-nd/4.0/.The final authenticated version is available online at:
http://dx.doi.org/10.1016/j.ijnonlinmec.2020.103591

(Article begins on next page)

16 October 2026

Progressive damage analysis of composite laminates subjected to low-velocity impact using 2D layer-wise structural models

M.H. Nagaraj, E. Carrera, M. Petrolo
MUL^2 Group, Department of Mechanical and Aerospace Engineering,
Politecnico di Torino, Corso Duca degli Abruzzi 24, 10129 Torino, Italy

Revised version of NLM-D-20-00213R1

Author for correspondence:
M. Petrolo
MUL^2 Group, Department of Mechanical and Aerospace Engineering,
Politecnico di Torino,
Corso Duca degli Abruzzi 24,
10129 Torino, Italy,
tel: +39 011 090 6845,
fax: +39 011 090 6899,
e-mail: marco.petrolo@polito.it

Abstract

The present work deals with the progressive damage analysis of composite laminates subjected to low-velocity impact. We develop a numerical model using higher-order structural theories based on the Carrera Unified Formulation (CUF) with Lagrange polynomials and resulting in a 2D refined layer-wise model. To model damage, we use a combination of the continuum damage-based CODAM2 intralaminar damage model to account for fiber and matrix damage within the ply, and cohesive elements to account for delamination between successive composite plies. We carry out numerical assessments for the case of a linear elastic composite plate subjected to impact, to compare the current framework with standard approaches based on 3D finite element (FE) analysis. We, then, consider the elastoplastic analysis of a bimetallic laminated plate to compare the performance of the proposed layer-wise model and 3D-FE approaches, for the case of nonlinear impact analysis. The final assessment considers progressive damage due to low-velocity impact, and the results are compared with available literature data. The numerical predictions show a good correlation with reference experimental and simulation results, thus validating the current framework for impact analysis of composite structures. Comparisons of the proposed layer-wise structural models with those based on 3D finite elements demonstrate the improved computational efficiency of the CUF models in terms of model size and analysis time.

Keywords: CUF, low-velocity impact, higher-order structural modeling, continuum damage mechanics

1 Introduction

Fibre-reinforced composites are a popular choice of engineering materials due to their superior mechanical properties, such as high specific strength and stiffness, resulting in light-weight structures. However, due to their layer-wise nature, composites tend to have fairly modest interlaminar properties making them quite vulnerable to transverse loads. An example is low-velocity impacts due to various events such as tool drop during maintenance or runway debris. Such events cause composite damage which may not be evident during a visual inspection and hence is termed as barely visible impact damage (BVID). Delamination is especially significant since it leads to a substantial reduction in structural stiffness. The issue of impact is thus a matter of high practical importance and needs to be taken into account in the design phase of the composite structure.

Several experimental investigations have been performed over the past few decades on the effect of impact on fibre-reinforced composites [1–4]. The high cost of such experimental campaigns motivates the development of computational tools to investigate the effects of impact loads on laminated composites. Numerical approaches to impact analysis of composite structures are generally classified based on the type of damage modelling used in the analysis. Fully discrete damage models employ interface elements, typically in the form of cohesive zone modelling (CZM), both within the ply to capture intralaminar matrix cracks, and between plies to capture delamination. For instance, Bouvet and co-workers developed a numerical model with discrete interface elements for low-velocity impact modelling [5, 6]. Discrete models have the advantage of being able to explicitly model the interaction between intralaminar matrix cracks and delamination, resulting in improved predictive capabilities [7]. Other works on the discrete modeling approach for low-velocity impact include [8–11]. Fully discrete models generally have high predictive accuracy, but at the cost of very high computational overheads, making such a modeling approach impractical for large-scale composite structures. A popular alternative to fully discrete modeling is the use of continuum damage mechanics (CDM) based material models to describe the intralaminar behaviour, while cohesive elements are applied between consecutive plies to account for delamination. This combined approach has a relatively lower computational cost compared to fully discrete approaches, while maintaining reasonable predictive accuracy, and making it a popular choice for the numerical modeling of laminated composites under impact loading. Several investigations on low-velocity impact using this approach have been reported in the literature, for instance, [12–16].

The progressive damage modelling of composites under impact is a computationally intensive task, and considerable efforts have been made in reducing the numerical cost. A common strategy is the use of single-step global/local approaches, where the impact area is discretized with a finer mesh relative to the global structural model. The two disparate meshes are often connected at the interface via tie constraints. Such a technique was used with a fully 3D-FE modeling approach in [17, 18]. A similar technique involving solid-shell coupling, where the global composite structure was modelled using shell elements while the impact region was modelled with solid elements, was used in [11].

The present work is motivated by the need for a computationally efficient numerical framework for the impact

analysis of composite structures. The numerical models used in this work utilise higher-order structural theories based on the Carrera Unified Formulation (CUF) [19], a hierarchical framework to generate 1D and 2D models with enhanced kinematics by the use of expansion functions over the cross-section and through the thickness, respectively. The use of kinematic enrichment functions results in refined beam and plate/shell models that can accurately evaluate 3D stress fields in a computationally efficient manner [20]. The current work is part of efforts towards the development of a CUF-based virtual test platform for the nonlinear analysis of composite structures. Previous works associated with this development include the nonlinear analysis of thin-walled structures [21, 22], micromechanical and multiscale analysis of composites [23, 24], delamination analysis of laminated composites [25], contact analysis of physically linear and nonlinear beams [26, 27], as well as progressive damage analysis of composite laminates [28], where composite damage is described via the CODAM2 intralaminar damage model [29–31]. The current work extends the works of [26–28] towards the development of a framework capable of performing impact analysis of fibre-reinforced composite structures. For the first time, in this paper, CUF models are evaluated for low-velocity impact, including a set of material nonlinearities.

The paper is divided as follows - Section 2 describes CUF and the development of higher-order structural theories. Section 3 discusses the implementation of the node-to-surface contact algorithm used in the present work. Numerical assessments on low-velocity impact are presented in Section 4, and finally the concluding remarks are given in Section 5.

2 Structural theories and FE formulation

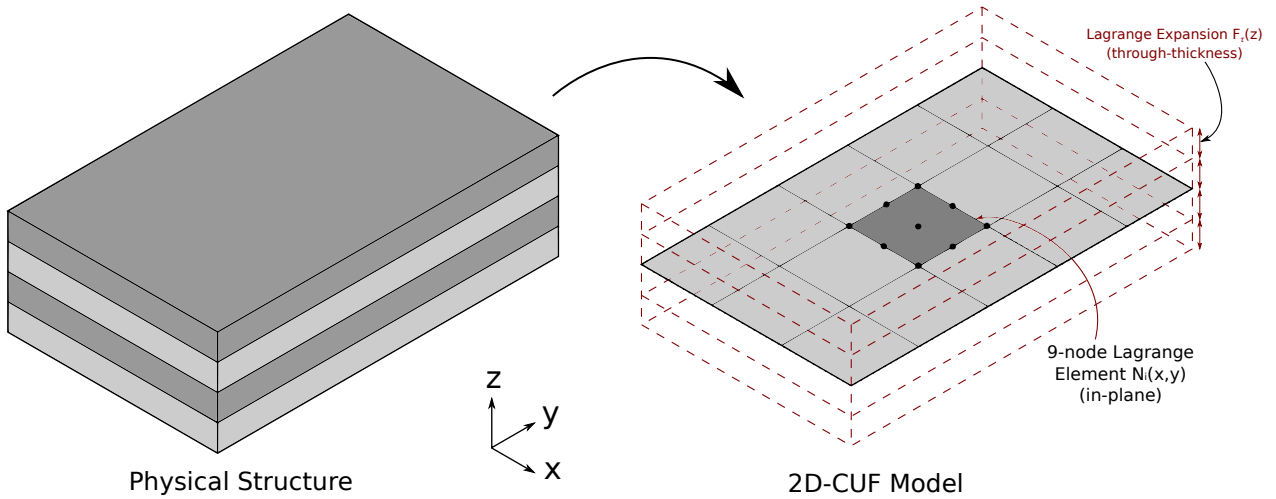

Figure 1: Layer-wise modelling of composite laminates in CUF

The structural modeling and FE formulation follow the same approach described in [28] in which a detailed explanation of the implementation of the CODAM2 material model and explicit time integration within the CUF framework can be found. Considering a general layered structure, such as that in Fig. 1, the layer-wise

2D CUF model defines the displacement field as

$$\mathbf{u}(x,y,z) = F_\tau(z)\mathbf{u}_\tau(x,y), \tau = 1,2,\dots M \tag{1}$$

where the expansion function $F_\tau(z)$ describes the kinematic approximation through the thickness of the plate, and $\mathbf{u}_\tau(x,y)$ are the generalized displacements. The choice of the expansion, F_τ, and the number of terms in the expansion, M, determines the structural theory used in the analysis and is a choice of the user. In the current work, 1D Lagrange polynomials are used as expansion functions through the thickness. According to CUF terminology, such a combination is referred to as the Lagrange-Expansion (LE) class. LE results in a layer-wise model, as shown in Fig. 1, with purely displacement degrees of freedom (DOF). A detailed explanation of the use of Lagrange polynomials as expansion functions can be found in [19].

2.1 Finite element formulation

The stress and strain fields are

$$\begin{aligned} \boldsymbol{\sigma} &= \{\sigma_{xx}, \sigma_{yy}, \sigma_{zz}, \sigma_{xy}, \sigma_{xz}, \sigma_{yz}\} \\ \boldsymbol{\varepsilon} &= \{\varepsilon_{xx}, \varepsilon_{yy}, \varepsilon_{zz}, \varepsilon_{xy}, \varepsilon_{xz}, \varepsilon_{yz}\} \end{aligned} \tag{2}$$

The linear strain-displacement relation is

$$\boldsymbol{\varepsilon} = \mathbf{D}\mathbf{u} \tag{3}$$

with the linear differential operator, $\mathbf{D}$, defined as

$$\mathbf{D} = \begin{bmatrix} \frac{\partial}{\partial x} & 0 & 0 \\ 0 & \frac{\partial}{\partial y} & 0 \\ 0 & 0 & \frac{\partial}{\partial z} \\ \frac{\partial}{\partial y} & \frac{\partial}{\partial x} & 0 \\ \frac{\partial}{\partial z} & 0 & \frac{\partial}{\partial x} \\ 0 & \frac{\partial}{\partial z} & \frac{\partial}{\partial y} \end{bmatrix}$$

The constitutive relation is

$$\boldsymbol{\sigma} = \mathbf{C}^{sec}\boldsymbol{\varepsilon} \tag{4}$$

where $\mathbf{C}^{sec}$ is the secant stiffness matrix depending on the material model used in the analysis. The current work uses the CODAM2 intralaminar damage model [29, 30]. The damaged stress state is then represented by $\boldsymbol{\sigma}$. The in-plane geometry is discretized using 2D quadrilateral finite elements (FE), using nodal interpolation functions $N_i(x,y)$, leading to the following 3D form of the displacement field

$$\mathbf{u}(x,y,z) = N_i(x,y)F_\tau(z)\mathbf{u}_{\tau i} \tag{5}$$

The semi-discrete balance of momentum is

$$\mathbf{M}\ddot{\mathbf{u}} = \mathbf{F}_{ext} - \mathbf{F}_{int} \tag{6}$$

where $\mathbf{M}$ is the mass matrix, and $\mathbf{F}_{ext}$ and $\mathbf{F}_{int}$ are the external and internal force vectors, respectively. The transient nonlinear problem is solved explicitly using the central difference time integration scheme [32]. The interlaminar damage is addressed via cohesive elements as detailed in [25].

2.2 Nonlinear shear response

The current work extends the previous implementation of the CODAM2 material model reported in [28] by taking into account the nonlinear in-plane shear response, as described in [33]. The in-plane shear constitutive formulation, before matrix damage initiation, is then modified as

$$\tau_{12} = \begin{cases} \frac{|\gamma_{12}|}{\gamma_{12}}\tau(|\gamma_{12}|), & \text{for } |\gamma_{12}| = \gamma_{12}^{*} \\ \frac{|\gamma_{12}|}{\gamma_{12}}G_{12}^{0}\langle|\gamma_{12}| - \gamma_{12}^{p}\rangle, & \text{for } |\gamma_{12}| < \gamma_{12}^{*} \end{cases} \tag{7}$$

where $\tau(|\gamma_{12}|)$ is the experimentally obtained nonlinear shear behaviour. G_{12}^{0} is the initial shear modulus and $\langle\cdot\rangle$ is the Macaulay operator. γ_{12}^{*} is the maximum shear strain over time and γ_{12}^{p} is the inelastic shear strain, which is computed as

$$\gamma_{12}^{p} = \gamma_{12}^{*} - \tau_{12}^{*}/G_{12}^{0} \tag{8}$$

where τ_{12}^{*} is the shear stress corresponding to γ_{12}^{*}. Matrix damage initiates once the failure initiation criterion reaches unity, i.e. $F_2 = 1.0$, and since only the elastic internal energy is responsible for the damage process, the elastic component of the shear strain is determined as follows

$$\gamma_{12}^{e} = \gamma_{12} - \gamma_{12}^{p}|_{F_2=1} \tag{9}$$

where $\gamma_{12}^{p}|_{F_2=1}$ is the inelastic shear strain at the onset of matrix damage. The equivalent transverse strain (see Eq. 19 of Ref. [28]) is then computed as

$$\varepsilon_{2}^{eq} = \sqrt{(\gamma_{12}^{e})^2 + (\varepsilon_{22})^2} \tag{10}$$

After matrix damage is initiated, the shear stress is computed as

$$\tau_{12} = R_{12}G_{12}^{0}(\gamma_{12} - \gamma_{12}^{p}|_{F_2=1}) \tag{11}$$

where $R_{12} = (1-\omega_1)(1-\omega_2)$ is the stiffness reduction factor computed using the damage variables ω_i.

3 Contact mechanics

3.1 Forward increment Lagrange multiplier

The current work enforces contact constraints via the forward increment Lagrange multiplier algorithm, based on the works of Carpenter et al. [34]. A modification is necessary to avoid singularity problems in a fully explicit analysis. The displacement constraints at time t_{n+1} are combined with Lagrange multipliers at time t_n. This process is referred to as the forward increment Lagrange multiplier approach and ensures the non-singularity of the system. Considering this approach, the incremental equation of motion is

$$\mathbf{M}\ddot{\mathbf{u}}_n + \mathbf{F}_{int}(\mathbf{u}_n, \dot{\mathbf{u}}_n) + \mathbf{G}_{n+1}^T \boldsymbol{\lambda}_n = \mathbf{F}_{ext} \tag{12}$$

subject to

$$\mathbf{G}_{n+1}\{\mathbf{u}_{n+1} + \mathbf{X}\} = \mathbf{0} \tag{13}$$

where $\mathbf{M}$ is the diagonalised mass matrix, $\mathbf{G}$ is the contact constraint matrix, $\mathbf{X}$ is the nodal position vector in the reference configuration, and $\boldsymbol{\lambda}$ is the vector of Lagrange multipliers. The central difference scheme is used for the explicit integration of Eq. 12, leading to

$$\mathbf{u}_{n+1} = \mathbf{u}_{n+1}^* + \mathbf{u}_{n+1}^c \tag{14}$$

where

$$\mathbf{u}_{n+1}^* = \Delta t^2 \mathbf{M}^{-1}[\mathbf{F}_{ext} - \mathbf{F}_{int}] + 2\mathbf{u}_n - \mathbf{u}_{n-1} \tag{15}$$

$$\boldsymbol{\lambda}_n = [\Delta t^2 \mathbf{G}_{n+1}\mathbf{M}^{-1}\mathbf{G}_{n+1}^T]^{-1}\mathbf{G}_{n+1}\{\mathbf{u}_{n+1}^* + \mathbf{X}\} \tag{16}$$

$$\mathbf{u}_{n+1}^c = -\Delta t^2 \mathbf{M}^{-1}\mathbf{G}_{n+1}^T \boldsymbol{\lambda}_n \tag{17}$$

For the incremental solution of Eqs. 14-17, a trial solution is first obtained for the incremental displacement, denoted by $\mathbf{u}_{n+1}^*$, where the effect of the contact forces $\boldsymbol{\lambda}$ are not considered. The updated position of the contact nodes ($\mathbf{x}_{n+1}^* = \mathbf{u}_{n+1}^* + \mathbf{X}$) is then determined, and, then, the penetration check is performed. The constraint matrix is assembled, and used in Eq. 16 to calculate the Lagrange multipliers, $\boldsymbol{\lambda}$, which have the physical meaning of contact forces. The incremental displacement due to contact is computed from Eq. 17, and the updated displacements are then determined using Eq. 14. Further details of the forward increment Lagrange multiplier approach within explicit time integration schemes can be found in [34].

3.2 Node-to-surface contact

The current work uses the Lagrange multiplier approach described in Section 3.1 in conjunction with node-to-surface contact discretisation of the contact surfaces. In such an approach, the target surface is discretised

using 2D contact patches while the surface of the contacting body is discretised with contact nodes, as shown in Fig. 2. The constraint matrix $\mathbf{G}$ then takes the following form

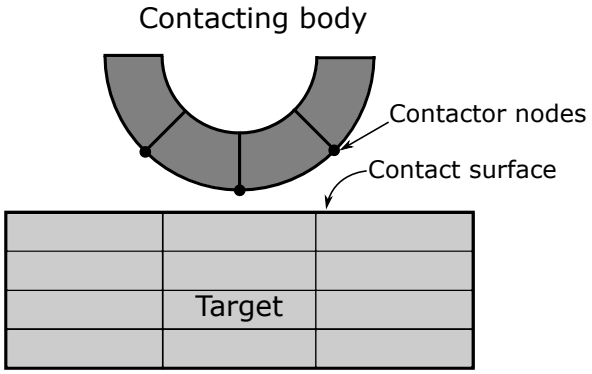

Figure 2: 2D schematic representation of node-to-surface contact discretisation

$$\mathbf{G} = \begin{bmatrix} N_1 & 0 & 0 & \dots & N_m & 0 & 0 & -1 & 0 & 0 \\ 0 & N_1 & 0 & \dots & 0 & N_m & 0 & 0 & -1 & 0 \\ 0 & 0 & N_1 & \dots & 0 & 0 & N_m & 0 & 0 & -1 \end{bmatrix} \tag{18}$$

where N and m are the nodal interpolation function and number of nodes of the contact surface element, respectively. The last three columns of $\mathbf{G}$ represent the constraints of the contact node DOF, for the node associated with the given contact surface element. Determining the contact point on the element surface, where the contact node penetrates the contact surface, is performed via closest point projection, described in [35, 36]. The constraint matrix thus assembled is used in Eq. 16 to determine the contact forces.

4 Numerical examples

4.1 Elastic impact in a square composite plate

The first numerical assessment involves the linear elastic analysis of a square composite plate. The motivation of this example is to compare standard modelling approaches, i.e. 3D-FE, with the proposed modelling approach based on 2D higher-order layer-wise theories; specifically, in terms of the model size and required analysis time for comparable accuracy of the stress field. The composite laminate is quasi-isotropic, with a ply stacking sequence of $[90/45/0/-45]_{2s}$ and ply thickness of 0.125 mm. The material system considered is an IM7/8552 carbon fibre reinforced polymer (CFRP), and its material properties are in Table 1. The composite plate is clamped at all four edges and subjected to a transverse impact at its centre via a 16 mm diameter spherical impactor with an initial velocity of 5 m/s. A schematic representation of the structure is in Fig. 3. The structural modelling of the composite plate adopts a series of 2D-CUF models, and, for verification purposes, 3D-FE models from ABAQUS/Explicit. The three ABAQUS models have 1,3 and 5 solid (C3D8R) elements to model the individual ply thickness, respectively. The CUF models consider increasing expansion orders to model each ply through its

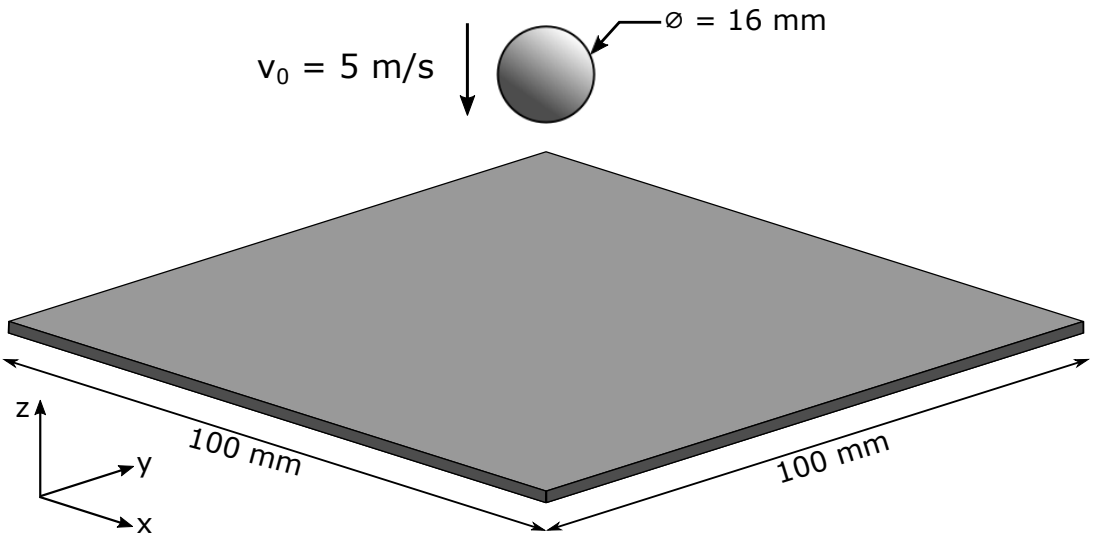

Figure 3: Schematic representation of the square $[90/45/0/-45]_{2s}$ quasi-isotropic composite plate under transverse low-velocity impact

Table 1: Material properties of the IM7/8552 CFRP system

E_1 [GPa]	E_2 [GPa]	E_3 [GPa]	G_{12} [GPa]	G_{13} [GPa]	G_{23} [GPa]	ν_{12}	ν_{13}	ν_{23}	ρ [kg/m^3]
165.00	9.00	9.00	5.60	5.60	2.80	0.34	0.34	0.50	1700.00

thickness, denoted as CUF - LEx, where x specifies the order of the Lagrange expansion; also, one CUF model uses three LE1 per each layer. Table 2 provides model information for the various numerical models, along with the computational size and analysis time. The ABQ-Coarse (1 element/ply) model is kinematically equivalent, through the thickness, to the CUF-LE1 (1 LE1/ply) model, while the same holds for the ABQ-Medium (3 elements/ply) and CUF-3LE1 (3 LE1/ply) models.

The in-plane normal stress σ_{xx} and shear stress σ_{xy}, through the laminate thickness at the point [x=48, y=48], are plotted in Fig. 4a and Fig. 4b, respectively. The interlaminar shear stress σ_{yz}, through the thickness at the point [x=40, y=40], is shown in Fig. 5. The points are in the impacted region as one of the aims of this section is to verify the capabilities of the structural models to detect stress fields where damage initiation could take place. The results suggest that

1. The in-plane stress components, as reported by the various numerical models, are in agreement with each other as seen in Fig. 4. As well-known, the proper detection of the in-plane components does not require the refinement of the structural model or the mesh.

2. Significant differences are visible, on the other hand, in the interlaminar shear stress σ_{yz}, plotted in Fig. 5. The use of a single solid element to model the ply thickness in 3D-FE does not result in accurate stress evaluation. A similar trend is present in the CUF model with a single linear expansion, i.e., CUF (1 LE1/ply). The use of higher-order thickness expansions, or multiple LE1 per layer, in CUF leads to a converged solution.

Table 2: Model information for the linear elastic stress analysis of the $[90/45/0/-45]_{2s}$ composite plate subjected to low-velocity impact

Model	Discretisation of the composite laminate	DOF	Analysis Time* [hh:mm:ss]
ABQ - Coarse	102,400 C3D8R (1 element/ply)	334,611	0:09:04
ABQ - Medium	307,200 C3D8R (3 elements/ply)	964,467	1:15:06
ABQ - Refined	512,000 C3D8R (5 elements/ply)	1,594,323	3:16:33
CUF - LE1	48 Q9 elements in-plane (1 LE1/ply)	10,659	0:10:29
CUF - LE2	48 Q9 elements in-plane (1 LE2/ply)	20,691	0:37:55
CUF - LE3	48 Q9 elements in-plane (1 LE3/ply)	30,723	1:30:46
CUF - 3LE1	48 Q9 elements in-plane (3 LE1/ply)	30,723	1:38:53

* The reported run-times are based on analyses performed on a desktop computer using a single core.

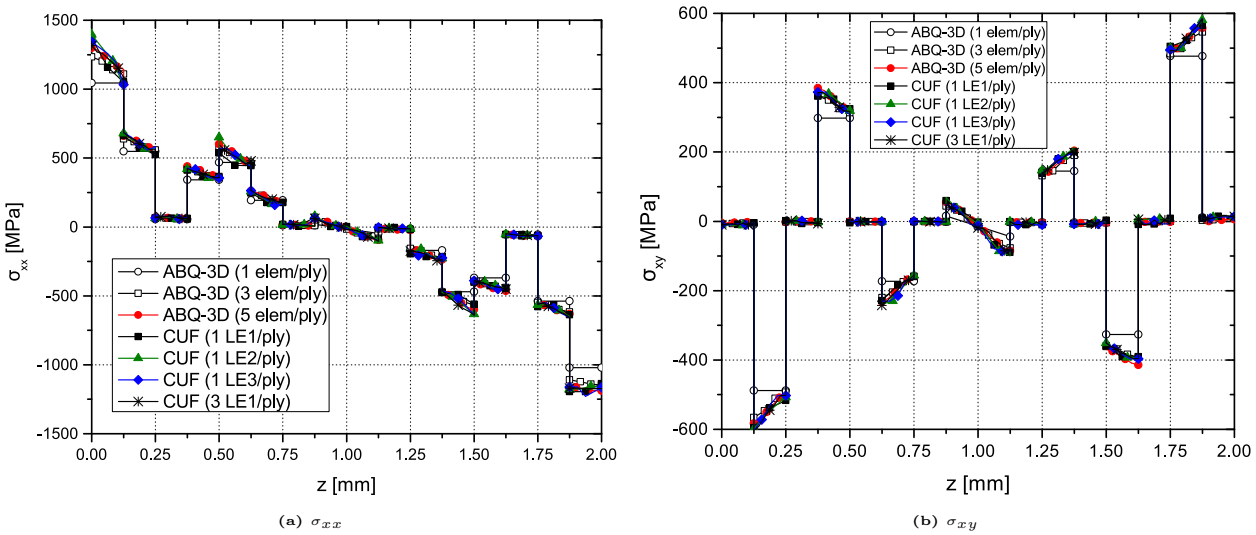

(a) σ_{xx} (b) σ_{xy}

Figure 4: In-plane stress components through the thickness of the square composite plate

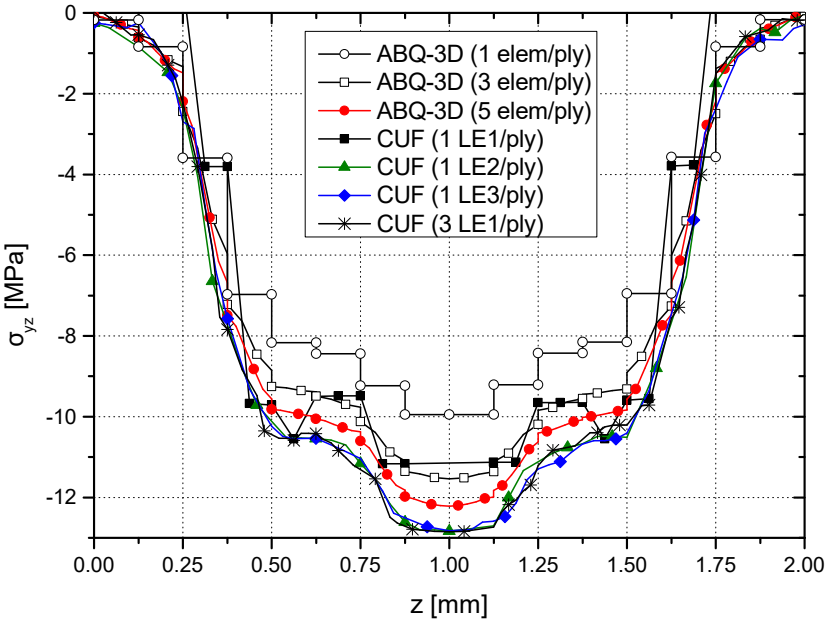

Figure 5: Interlaminar shear stress σ_{yz} through the thickness of the square composite plate

3. Increasing the number of elements through the thickness in the 3D-FE models results in stress fields approaching that of the converged CUF results. This is in line with the findings reported in [20].

4. The accurate evaluation of the 3D stress field is significant since it constitutes an input for composite damage models, in the case of a fully nonlinear progressive damage analysis. Inaccurate stress field predictions due to limitations of the structural model can significantly influence failure initiation and propagation.

5. Although the stress fields were obtained via the constitutive law, an almost perfect continuity was achieved at the interfaces.

6. In the case of the CUF models, the coarsest mesh, which results in converged interlaminar stresses is the CUF-LE2 model, with a single quadratic expansion (LE2) per ply of the laminate. This model requires about $76x$ fewer DOF and achieves over a $5x$ speed-up in analysis time, compared to the refined ABAQUS model, for comparable quality of results. The speed-up in analysis time may be higher. The current values are most likely due to differences in the implementation of the contact algorithm. In fact, in purely linear cases or nonlinear cases with no contact, significantly higher speed-ups were achieved [24, 37].

4.2 Elastoplastic analysis of bimetallic laminated plate

The objective of the current numerical assessment is to evaluate CUF layer-wise models' performance, compared to 3D-FEA, for the case of nonlinear impact analysis. Metal plasticity is considered as the source of material nonlinearity. The structure presented previously in Section 4.1 (Fig. 3) is considered, but, in the present analysis, the plate is a bimetallic 16-layer laminate, composed of two materials M1 and M2 whose elastoplastic properties

are listed in Table 3. The stacking sequence of the metal laminate is $[M1/M2]_{4s}$. The metallic constituents are assumed to be elastic-perfectly plastic. The plate is impacted at its center by a spherical impactor of diameter 16 mm, with an initial velocity of 5 m/s. The impact problem is analyzed using CUF layer-wise models, and reference solutions are obtained using 3D-FEA in ABAQUS/Explicit. Details of the models developed with the two approaches are presented in Table 4. The vertical deflection u_z and the equivalent plastic strain, along the y-axis at the impact surface of the bimetallic plate, are plotted in Fig. 6 and Fig. 7, respectively. The 3D distribution of equivalent plastic strain at the impact site is shown in Fig. 8. The results indicate that

1. The deformation predicted by the CUF model is in good agreement with 3D-FE models, as seen in Fig. 6. For the case of 3D-FE, insufficient mesh refinement leads to errors in the predicted deformation.

2. As seen in Fig. 7 and Fig. 8, the current approach is able to accurately quantify the extent as well as the morphology of the plastic zone.

3. The CUF model requires approximately $80x$ fewer degrees of time and provides over a $3.6x$ speed-up in analysis time, for comparable quality of results.

Table 3: Material properties of the elastoplastic materials used for the bimetallic plate

Material	Young's Modulus E [GPa]	Poisson's ratio ν [-]	Yield stress σ_y [MPa]
Material-1 (M1)	210.0	0.3	210.0
Material-2 (M2)	70.0	0.3	110.0

Table 4: Model information for the elastoplastic analysis of the bimetallic plate subjected to low-velocity impact

Model	Discretisation of the bimetallic plate	DOF	Analysis Time* [hh:mm:ss]
ABQ - Coarse	102,400 C3D8R (1 element/layer)	334,611	00:24:18
ABQ - Refined	270,848 C3D8R (2 elements/layer)	856,251	01:55:12
CUF-LW	48 Q9 elements in-plane (1 LE1/layer)	10,659	0:31:29

* The reported run-times are based on analyses performed on a desktop computer using a single core.

4.3 Progressive damage analysis of a circular plate

This numerical assessment consists of the progressive damage analysis of a circular composite plate subjected to a transverse low-velocity impact. The study is based on [14], which provides reference experimental and numerical results. A schematic representation of the structure is in Fig. 9. The material is an HTS40/9772 unidirectional CFRP, and its properties are in Table 5. The laminate consists of a $[0/90]_{2s}$ stacking sequence with a ply thickness of 0.25 mm, leading to a laminate thickness of 2.0 mm. The laminate is fully clamped at all edge nodes. The impactor is a rigid sphere of diameter 15 mm, with an initial prescribed velocity $v_0 = 3.83$

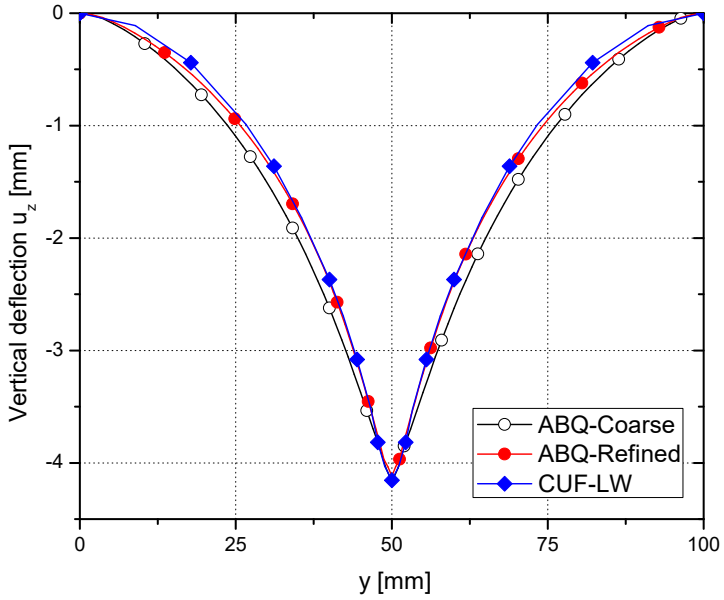

Figure 6: Vertical deflection u_z along the y-axis at the impact surface of the bimetallic plate

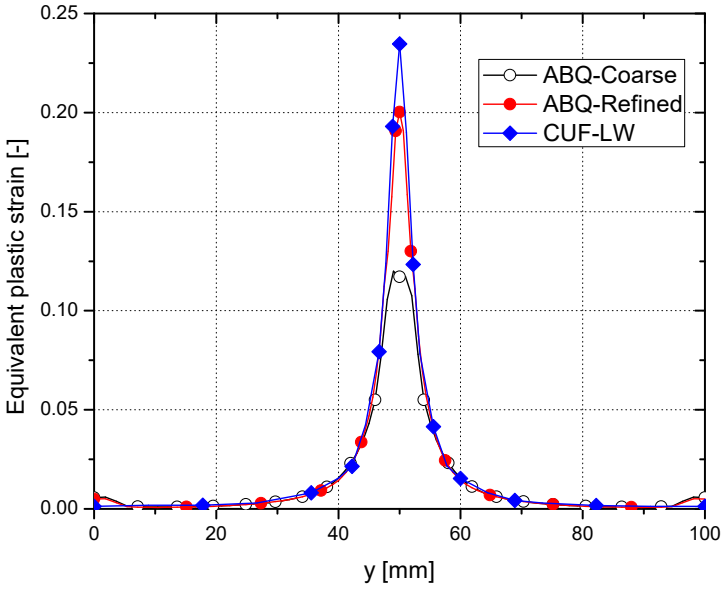

Figure 7: Equivalent plastic strain along the y-axis at the impact surface of the bimetallic plate

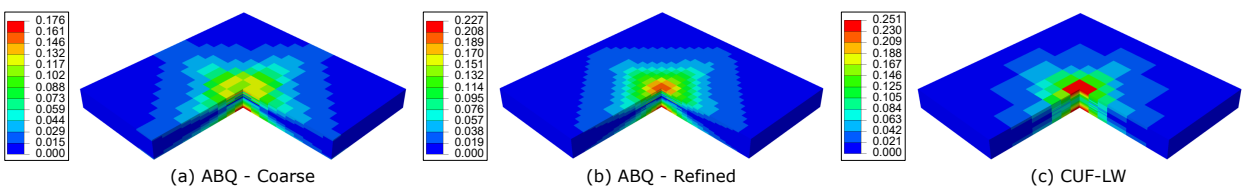

Figure 8: Distribution of the equivalent plastic strain at the impact site of the bimetallic plate

m/s, and kinetic energy of 7.35 J. The numerical models adopted CUF models with a varying level of in-plane

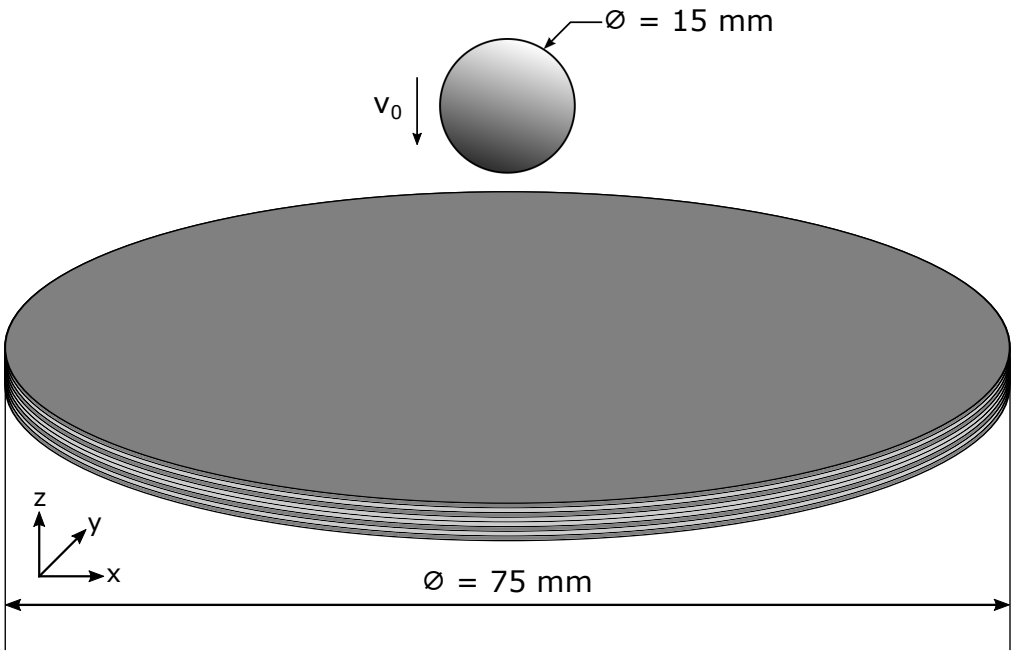

Figure 9: Schematic representation of the $[0/90]_{2s}$ composite plate under transverse low-velocity impact by a spherical indenter with a kinetic energy of 7.35 J

Table 5: Properties of the HTS40/9772 unidirectional CFRP material system [14]

E_1 [GPa]	E_2 [GPa]	E_3 [GPa]	G_{12} [GPa]	G_{13} [GPa]	G_{23} [GPa]	ν_{12}	ν_{13}	ν_{23}	Density $[kg/m^3]$
153.0	10.3	10.3	6.0	6.0	3.7	0.3	0.3	0.4	1600.0
X_T [MPa]	X_C [MPa]	Y_T [MPa]	Y_C [MPa]	S_{12} [MPa]	S_{23} [MPa]	G_1^T $[kJ/m^2]$	G_2^T $[kJ/m^2]$	G_1^C $[kJ/m^2]$	G_2^C $[kJ/m^2]$
2537.0	1580.0	82.0	236.0	90.0	40.0	91.6	0.22	79.9	1.1

Table 6: Properties of the cohesive layer [14]

Property	Mode I	Mode II	Mode III
Elastic modulus [GPa/mm]	1373.3	493.3	493.3
Interlaminar strength [MPa]	62.3	92.3	92.3
Interlaminar fracture toughness $[kJ/m^2]$	0.28	0.79	0.79

mesh refinement and through-thickness expansions, to investigate their effects on the accuracy of the numerical predictions. Delamination is included via cohesive elements between successive plies, adopting the mixed-mode cohesive constitutive model described in [38]. Further details on the development and FE formulation of the cohesive element in the CUF framework are in [25]. The properties of the cohesive layer are in Table 6. Model data related to the discretization used and computational costs are in Table 7. As a representative example, the in-plane discretization of the CUF model with 192 Q9 elements is in Fig. 10. The first study investigates the influence of the in-plane discretization on the quality of the results. A quadratic (LE2) ply thickness expansion

Table 7: Details of the structural models used for the progressive damage analysis of the $[0/90]_{2s}$ composite plate subjected to transverse low-velocity impact

Model	Discretisation of the composite laminate	DOF	Analysis Time* [hh:mm:ss]
CUF - 132 Q9/LE2	132 Q9 elements in-plane (1 LE2/ply)	39,816	5:13:44
CUF - 192 Q9/LE1	192 Q9 elements in-plane (1 LE1/ply)	38,448	6:45:13
CUF - 192 Q9/LE2	192 Q9 elements in-plane (1 LE2/ply)	57,672	8:46:22
CUF - 192 Q9/LE3	192 Q9 elements in-plane (1 LE3/ply)	76,896	11:37:57
CUF - 260 Q9/LE2	260 Q9 elements in-plane (1 LE2/ply)	77,832	11:49:58

* The reported run-times are based on analyses performed on a desktop computer using 6 cores.

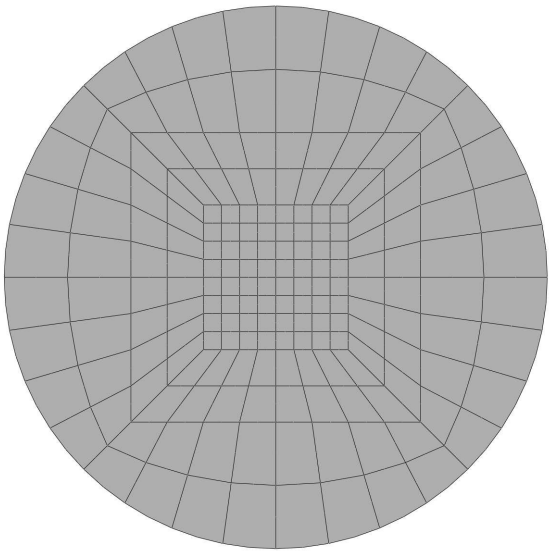

Figure 10: Schematic representation of the 192 Q9 in-plane discretisation used for the $[0/90]_{2s}$ circular composite plate

function is considered in all cases. The impact force-time curves for the considered CUF models are in Fig. 11. Based on the results of the in-plane mesh convergence study, the 192 Q9 mesh (see Fig. 10) is selected for further investigations. The next study considers the influence of the thickness expansion function on the accuracy of the result. The structural models have linear (LE1), quadratic (LE2), and cubic (LE3) ply thickness expansion functions. The impact force-time curves obtained with these models are plotted in Fig. 12. Reference experimental and simulation curves obtained from [14] are reported in all cases for comparison. Contour plots of the damage variables after impact, for the case of the 192 Q9 - LE3 model, are in Fig. 13, and the predicted delamination at the ply interfaces in Fig. 14.

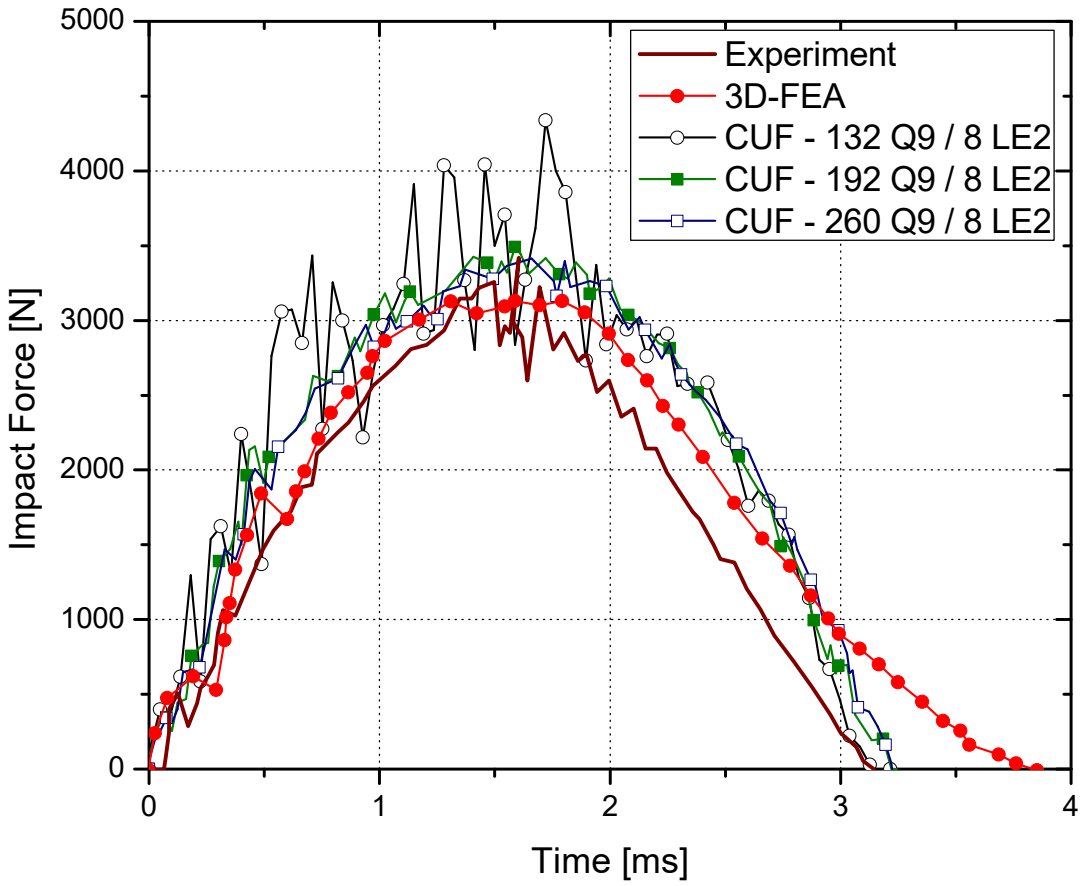

Figure 11: In-plane mesh effect of the impact force-time response for the $[0/90]_{2s}$ circular composite plate. Reference experimental and numerical data from [14]

The results suggest that

1. The use of linear expansions (LE1) results in significant oscillations. Progressive refinement through the thickness using LE2 and LE3 functions results in a smoother and more accurate global response. Based on the results from Section 4.1, the beneficial influence of higher-order thickness functions confirms the importance of accurate transverse shear stresses.

2. The numerically predicted morphology of the damage, see Fig. 14, shows a good agreement with [14] in which Figs. 8 (a) and (b) show experimental and numerical delaminated zones. Likewise, the morphologies

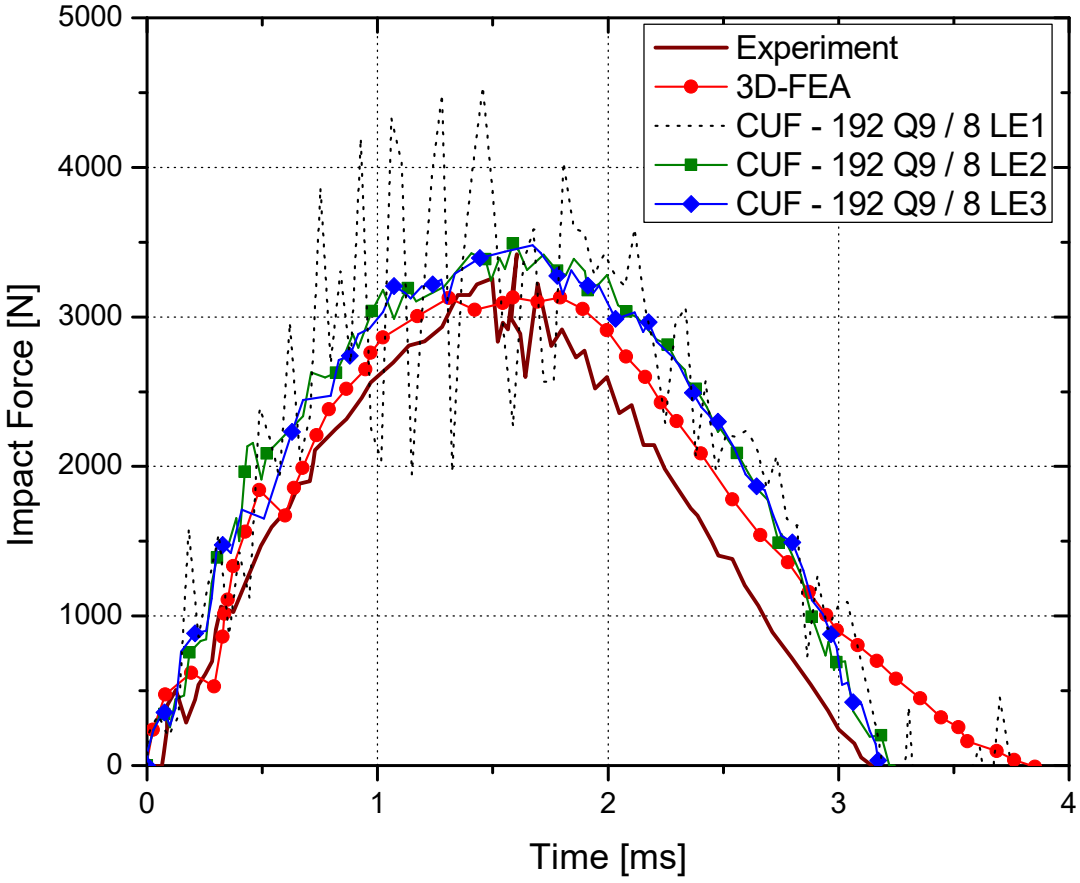

Figure 12: Through-thickness expansion effect on the impact force-time response for the $[0/90]_{2s}$ circular composite plate. Reference experimental and numerical data from [14].

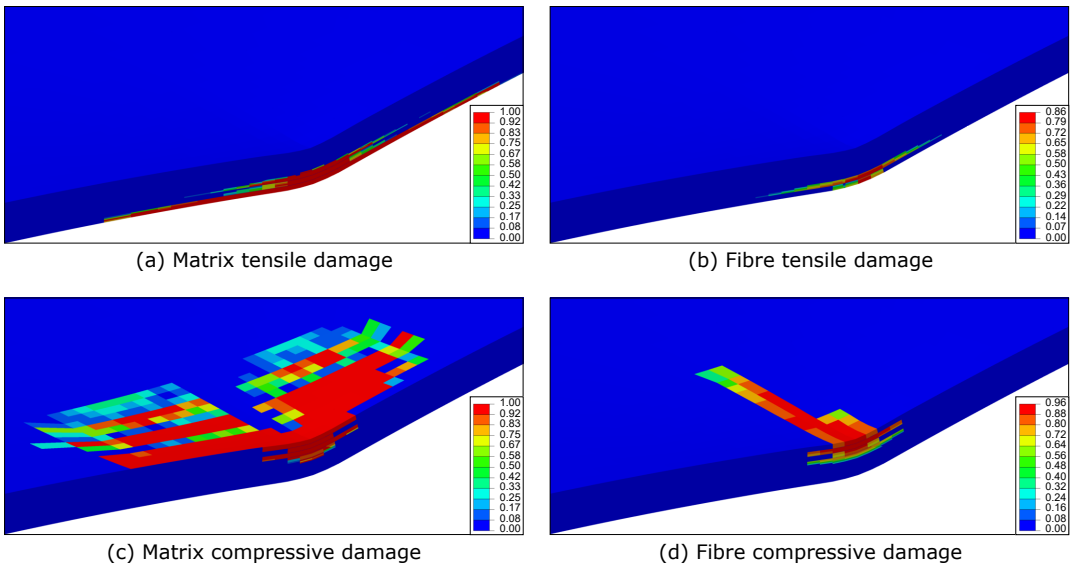

Figure 13: Predicted damage at the impact region of the $[0/90]_{2s}$ circular composite plate

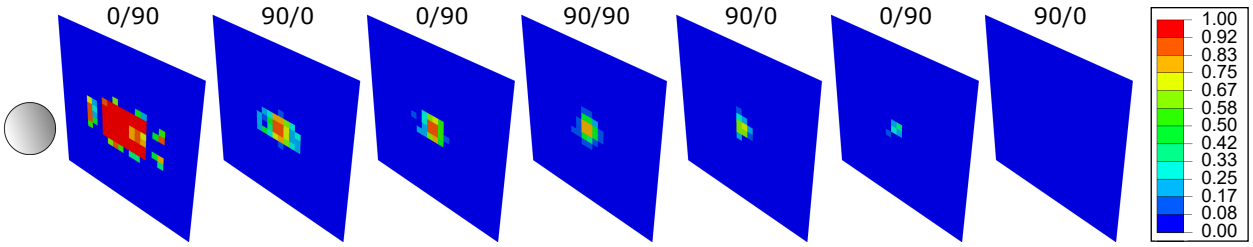

Figure 14: Predicted delamination at the ply interfaces of the $[0/90]_{2s}$ circular composite plate

of different damage mechanisms in Fig. 13 are in good agreement with Figs. 10(a) and 10(b) of [14].

3. The difference between the experimental and converged CUF results in the unloading phase is attributed to the fact that the CUF models do not consider friction at the contact interfaces or account for plastic indentations of the laminate at the impact zone, both of which are mechanisms for energy dissipation. Nevertheless, a good general agreement is observed between experimental and CUF curves, including the accurate prediction of the peak load.

4. One of the advantages provided by the proposed layer-wise scheme is the direct modelling of the damage states at each layer. The predicted damage state shows significant saturated matrix damage, with a small amount of unsaturated fibre damage. This indicates that matrix damage is the primary energy dissipation mechanism within the laminate.

5 Conclusions

The objective of the current work is the development of a novel numerical framework based on higher-order structural theories for the impact analysis of composite structures. The Carrera Unified Formulation is used to generate 2D layer-wise structural models. Each ply of the laminate is explicitly modelled using Lagrange polynomial-based thickness expansion functions. The intralaminar composite damage is modelled using the CODAM2 material model, and delamination at the ply interface is taken into account using cohesive elements based on a mixed-mode cohesive constitutive law. Numerical assessments were first performed considering the linear elastic material behaviour to compare the stress predictions of the CUF layer-wise models with that of the standard approach, i.e., 3D-FE. The next assessment was the elastoplastic analysis of a bimetallic laminated plate, to compare the performance of CUF and 3D-FE models for nonlinear impact analysis. The final numerical assessment was the progressive damage analysis of a $[0/90]_{2s}$ circular composite plate composed of HTS40/9772 unidirectional carbon fibre reinforced polymer. The main conclusions drawn from the present work are the following:

1. The proposed numerical framework based on layer-wise 2D-CUF theories can accurately simulate composite laminates subjected to impact loads, as verified concerning reference 3D-FE.

2. 3D-FE models require expensive meshes due to the necessity of fine through the thickness discretization and aspect ratio constraints. The detection of the interlaminar stress is particularly demanding. 2D CUF models enrich the kinematics through the thickness and, having just in-plane aspect ratio constraints, can deliver accurate predictions with one- to a two-fold reduction of DOF.

3. CUF layer-wise models are demonstrated to have significant computational efficiency, compared to 3D-FE models, for the case of nonlinear impact analysis.

4. The progressive damage analysis of composite laminates subjected to low-velocity impact, performed using the present approach, shows a good agreement with experimental reference results and numerical predictions reported in the literature, thus validating the proposed framework for such a class of problems.

The presented results constitute preliminary investigations of the analysis of composite structures under low-velocity impact using CUF. Future works include further implementations such as frictional contact to improve the predictive capabilities of the numerical framework and the use of global/local and adaptive cohesive layer insertion techniques to reduce the computational costs.

Acknowledgements

This research work has been carried out within the project ICONIC (Improving the Crashworthiness of Composite Transportation Structures), funded by the European Union Horizon 2020 Research and Innovation program under the Marie Skłodowska-Curie Grant agreement No. 721256.

References

[1] WJ Cantwell and J Morton. Comparison of the low and high velocity impact response of CFRP. *Composites*, 20(6):545–551, 1989.

[2] HY Choi, RJ Downs, and F Chang. A new approach toward understanding damage mechanisms and mechanics of laminated composites due to low-velocity impact: Part I—experiments. *Journal of Composite Materials*, 25(8):992–1011, 1991.

[3] T Anderson and E Madenci. Experimental investigation of low-velocity impact characteristics of sandwich composites. *Composite structures*, 50(3):239–247, 2000.

[4] CS Lopes, O Seresta, Y Coquet, Z Gürdal, PP Camanho, and B Thuis. Low-velocity impact damage on dispersed stacking sequence laminates. Part i: experiments. *Composites Science and Technology*, 69(7-8):926–936, 2009.

[5] C Bouvet, B Castanié, M Bizeul, and J Barrau. Low velocity impact modelling in laminate composite panels with discrete interface elements. *International Journal of Solids and Structures*, 46(14-15):2809–2821, 2009.

[6] C Bouvet, S Rivallant, and J Barrau. Low velocity impact modeling in composite laminates capturing permanent indentation. *Composites Science and Technology*, 72(16):1977–1988, 2012.

[7] XC Sun, MR Wisnom, and SR Hallett. Interaction of inter-and intralaminar damage in scaled quasi-static indentation tests: Part 2–numerical simulation. *Composite Structures*, 136:727–742, 2016.

[8] L Lammerant and I Verpoest. Modelling of the interaction between matrix cracks and delaminations during impact of composite plates. *Composites Science and Technology*, 56(10):1171–1178, 1996.

[9] MFSF De Moura and JPM Gonçalves. Modelling the interaction between matrix cracking and delamination in carbon–epoxy laminates under low velocity impact. *Composites Science and Technology*, 64(7-8):1021–1027, 2004.

[10] Y Shi, C Pinna, and C Soutis. Modelling impact damage in composite laminates: a simulation of intra-and inter-laminar cracking. *Composite Structures*, 114:10–19, 2014.

[11] XC Sun and SR Hallett. Barely visible impact damage in scaled composite laminates: Experiments and numerical simulations. *International Journal of Impact Engineering*, 109:178–195, 2017.

[12] A Forghani and R Vaziri. Computational modeling of damage development in composite laminates subjected to transverse dynamic loading. *Journal of Applied Mechanics*, 76(5):051304, 2009.

[13] EV González, P Maimí, PP Camanho, A Turon, and JA Mayugo. Simulation of drop-weight impact and compression after impact tests on composite laminates. *Composite Structures*, 94(11):3364–3378, 2012.

[14] Y Shi, T Swait, and C Soutis. Modelling damage evolution in composite laminates subjected to low velocity impact. *Composite Structures*, 94(9):2902–2913, 2012.

[15] D Feng and F Aymerich. Finite element modelling of damage induced by low-velocity impact on composite laminates. *Composite Structures*, 108:161–171, 2014.

[16] W Tan, BG Falzon, LNS Chiu, and M Price. Predicting low velocity impact damage and Compression-After-Impact (cai) behaviour of composite laminates. *Composites Part A: Applied Science and Manufacturing*, 71:212–226, 2015.

[17] A Riccio, A De Luca, G Di Felice, and F Caputo. Modelling the simulation of impact induced damage onset and evolution in composites. *Composites Part B: Engineering*, 66:340–347, 2014.

[18] F Caputo, A De Luca, G Lamanna, V Lopresto, and A Riccio. Numerical investigation of onset and evolution of LVI damages in carbon–epoxy plates. *Composites Part B: Engineering*, 68:385–391, 2015.

[19] E Carrera, M Cinefra, M Petrolo, and E Zappino. *Finite element analysis of structures through unified formulation.* John Wiley & Sons, 2014.

[20] AG de Miguel, I Kaleel, MH Nagaraj, A Pagani, M Petrolo, and E Carrera. Accurate evaluation of failure indices of composite layered structures via various FE models. *Composites Science and Technology*, 167:174–189, 2018.

[21] A Pagani and E Carrera. Unified formulation of geometrically nonlinear refined beam theories. *Mechanics of Advanced Materials and Structures*, 25(1):15–31, 2018.

[22] M Petrolo, MH Nagaraj, I Kaleel, and E Carrera. A global-local approach for the elastoplastic analysis of compact and thin-walled structures via refined models. *Computers & Structures*, 206:54–65, 2018.

[23] I Kaleel, M Petrolo, AM Waas, and E Carrera. Micromechanical progressive failure analysis of fiber-reinforced composite using refined beam models. *Journal of Applied Mechanics*, 85(2):021004, 2018.

[24] I Kaleel, M Petrolo, E Carrera, and AM Waas. Computationally efficient concurrent multiscale framework for the nonlinear analysis of composite structures. *AIAA Journal*, 57(9):4029–4041, 2019.

[25] I Kaleel, E Carrera, and M Petrolo. Progressive delamination of laminated composites via 1D models. *Composite Structures*, 235:111799, 2020.

[26] MH Nagaraj, I Kaleel, E Carrera, and M Petrolo. Contact analysis of laminated structures including transverse shear and stretching. *European Journal of Mechanics-A/Solids*, page 103899, 2019.

[27] MH Nagaraj, I Kaleel, E Carrera, and M Petrolo. Nonlinear analysis of compact and thin-walled metallic structures including localized plasticity under contact conditions. *Engineering Structures*, page 109819, 2019.

[28] MH Nagaraj, J Reiner, R Vaziri, E Carrera, and M Petrolo. Progressive damage analysis of composite structures using higher-order layer-wise elements. *Composites Part B: Engineering*, page 107921, 2020.

[29] A Forghani, N Zobeiry, A Poursartip, and R Vaziri. A structural modelling framework for prediction of damage development and failure of composite laminates. *Journal of Composite Materials*, 47(20-21):2553–2573, 2013.

[30] A Forghani, A Poursartip, and R Vaziri. An orthotropic non-local approach to modeling intra-laminar damage progression in laminated composites. *International Journal of Solids and Structures*, 180:160–175, 2019.

[31] J Reiner, T Feser, D Schueler, M Waimer, and R Vaziri. Comparison of two progressive damage models for studying the notched behavior of composite laminates under tension. *Composite Structures*, 207:385–396, 2019.

[32] R De Borst, MA Crisfield, JJC Remmers, and CV Verhoosel. *Nonlinear finite element analysis of solids and structures*. John Wiley & Sons, 2012.

[33] M. Shahbazi. *An efficient virtual testing framework to simulate the progression of damage in notched composite laminates*. PhD thesis, University of British Columbia, 2017.

[34] NJ Carpenter, RL Taylor, and MG Katona. Lagrange constraints for transient finite element surface contact. *International Journal for Numerical Methods in Engineering*, 32(1):103–128, 1991.

[35] JO Hallquist, GL Goudreau, and DJ Benson. Sliding interfaces with contact-impact in large-scale lagrangian computations. *Computer Methods in Applied Mechanics and Engineering*, 51(1-3):107–137, 1985.

[36] DJ Benson and JO Hallquist. A single surface contact algorithm for the post-buckling analysis of shell structures. *Computer Methods in Applied Mechanics and Engineering*, 78(2):141–163, 1990.

[37] SE Stapleton, B Stier, S Jones, A Bergan, I Kaleel, M Petrolo, E Carrera, and BA Bednarcyk. A critical assessment of design tools for stress analysis of adhesively bonded double lap joints. *Mechanics of Advanced Materials and Structures*, In Press.

[38] PP Camanho, CG Davila, and MF De Moura. Numerical simulation of mixed-mode progressive delamination in composite materials. *Journal of composite materials*, 37(16):1415–1438, 2003.